Physics Letters A 457 (2023) 128578

Contents lists available at ScienceDirect

Physics Letters A

journal homepage: www.elsevier.com/locate/pla

Effects of tilted Dirac cones and in-plane electric field on the valley-dependent magneto-optical absorption spectra in monolayer 8–*Pmmn* borophene

Ta T. Tho [a], Nguyen N. Hieu [b,c], Doan M. Quang [d], Nguyen Q. Bau [d,*], Bui D. Hoi [e,f,**]

[a] Department of Physics, Faculty of Mechanical Engineering, Hanoi University of Civil Engineering, Hanoi 100000, Viet Nam
[b] Institute of Research and Development, Duy Tan University, Da Nang 550000, Viet Nam
[c] Faculty of Natural Sciences, Duy Tan University, Da Nang 550000, Viet Nam
[d] Department of Theoretical Physics, Faculty of Physics, University of Science, Vietnam National University, Hanoi, 334 Nguyen Trai, Thanh Xuan, Hanoi 100000, Viet Nam
[e] Faculty of Physics, University of Education, Hue University, Hue 530000, Viet Nam
[f] Center for Theoretical and Computational Physics, University of Education, Hue University, Hue 530000, Viet Nam

ARTICLE INFO

Article history:
Received 20 October 2022
Received in revised form 21 November 2022
Accepted 2 December 2022
Available online 8 December 2022
Communicated by M.Z. Wu

Keywords:
Magneto-optical absorption
Valley polarization
Valleytronic
Borophene
2D Dirac material

ABSTRACT

We investigate the optical absorption properties in a 8-*Pmmn* borophene monolayer with anisotropic tilted Dirac cones, subjected to a perpendicular magnetic field and in-plane dc electric field (EF). Numerical results for the magneto-optical absorption coefficient (MOAC) show that the tilt of the Dirac cones causes the redshift of absorption peaks. More interestingly, there appears minor absorption peaks corresponding to the transitions between the Landau levels (LLs) n and $n \pm 2$ beside the principal maxima corresponding to the transitions between LLs n and $n \pm 1$. These minor peaks are absent in other two-dimensional Dirac materials with non-titled Dirac cones. The simultaneous presence of in-plane EF and the tilt parameter in 8–*Pmmn* borophene lifts the valley degeneracy in the LLs and causes the valley polarization in the MOAC, that do not occur in the absence of in-plane EF and/or the tilt parameter. The valley-polarized MOAC opens up potential applications in valleytronics.

1. Introduction

Since the discovery of graphene with outstanding physical properties opening a new era of materials science [1], scientists have been searching for other two-dimensional (2D) materials both theoretically and experimentally with perfect physical properties overcoming the disadvantages of graphene, that is the zero band gap which limits its applications in logic devices [2]. Accordingly, a variety of materials belonging to the 2D family have been discovered in turn, such as silicene [3,4], germanene [3,5], stanene [3,6,7] and then molybdenum disulfide [8], aluminene [9], arsenence [10], antimonene [11], bismuthene [12], phosphorene [13–15], and so on.

Borophene is a 2D lattice of boron atoms first predicted theoretically in the mid-1990 [16] and then experimentally successfully fabricated more than one decade later on Ag(111) substrates [17–23]. The synthesized structures exhibit many interesting physical properties including strong anisotropy that gives rise to anisotropic electrical, magnetic, thermal, and optical properties [24]. Thermodynamically, since the valence electrons of the boron atoms are less than the valence electrons of the carbon atoms in graphene, the 2D boron sheet is less stable than graphene, however this can be solved by increase the number of boron atoms [17,18]. Depending on the arrangements of the added boron atoms, we have different allotropes [25,26]. Most allotropes of borophene exhibit metallicity [25,26,19]. Others are proven to be semi-metallic with anisotropic Dirac cones, such as *Pmmn* borophene and *P*6/*mmm* borophene [27,28]. Among the pristine allotropes, 8–*Pmmn* borophene is of particular interest because it has anisotropic tilted Dirac cones and is one of the most stable structures [27]. The origin of the tilt in its energy dispersion has been suggested and discussed in some previous works [29–31]. 8–*Pmmn* borophene has been proven to possess many fascinating transport properties such as anisotropic plasmons, Friedel oscillations, undamped plasmon mode at high en-

* Corresponding author.
** Corresponding author at: Faculty of Physics, University of Education, Hue University, Hue 530000, Viet Nam.
E-mail addresses: nguyenquangbau@hus.edu.vn (N.Q. Bau), buidinhhoi@hueuni.edu.vn (B.D. Hoi).

https://doi.org/10.1016/j.physleta.2022.128578
0375-9601/

ergies, oblique Klein tunneling, Weiss oscillation in the magneto-conductivity, and direction-dependent optical conductivity [32–35].

Along with the widespread development of 2D materials, their optical absorption properties as well as 2D Dirac materials have been extensively studied. The tilt and anisotropy of Dirac cones would give rise to valley- and direction-dependent behaviors [33–36] including interesting optical transitions that are absent in normal (non-tilted) Dirac cones as shown, for instance, in Ref. [37]. However, the effect of a uniform static magnetic field was not included therein. On the other hand, the quantization of the energy band into Landau levels in the presence of a magnetic field is the origin of many magnetic field-induced effects such as the quantum Hall effect, cyclotron resonance, Shubnikov - de Haas oscillations, and so on. Recently, the magneto-optical absorption and transport properties have been studied in normal Dirac materials such as graphene [38], silicene and germanene [39], phosphorene [40], transition-metal dichalcogenides (TMDs) monolayers [41–43], and so on. The observations in these works show that the optical transitions are allowed only between adjacent LLs governing by the selection rules resulted from the electron wave functions in the optical transition matrix element. However, the study of magneto-optical absorption properties of materials with titled Dirac cones is still limited. The tilt of the Dirac cones is believed to modify the Landau levels and electron wave functions and expected to result in novel optical transitions that are absent in materials with non-tilted Dirac cones. Moreover, the role of valley degrees of freedom in tilted Dirac cones materials becomes more pronounced and the valley-dependent optical absorption can give potential applications in valleytronic devices.

In this work, we theoretically investigate the optical absorption properties in a 8–*Pmmn* borophene monolayer with the tilted and anisotropic Dirac cones, in the presence of a perpendicular uniform magnetic field and an in-plane dc electric field. We derive analytical expressions for the magneto-optical absorption coefficient (MOAC) by using the perturbation theory. In particular, we focus on the effect of the tilt of the Dirac cones on the absorption spectra. The paper is structured as follows. In the next section (Sec. 2), we present briefly the theoretical model and the derivation of the MOAC. Numerical results and discussion are given in Sec. 3. Finally, important conclusions are given in Sec. 4.

2. Theoretical framework

2.1. A 8–Pmmn borophene monolayer in crossed electric and magnetic field

In this investigation, we consider a monolayer of 8–*Pmmn* borophene lying in the $x-y$ plane as shown in Fig. 1. The energy dispersion of carriers (electrons and holes) around the Dirac points in the system forms anisotropic tilted Dirac cones, resulting from the following Hamiltonian [35,44]

$$H = \xi\left(v_x p_x \sigma_x + v_y p_y \sigma_y + v_t p_y \mathbb{1}\right), \tag{1}$$

where $\xi = +(-)$ refers to valley $K(K')$, $\vec{p} = (p_x, p_y)$ is the 2D carrier momentum, $\sigma = (\sigma_x, \sigma_y)$ and $\mathbb{1}$ are the pseudo Pauli matrices and the identity matrix, respectively. $\{v_x, v_y, v_t\} = \{0.86v_0, 0.69v_0, 0.32v_0\}$ are the velocity components with $v_0 = 10^6$ m s^{-1}. Note that the nonzero v_t in the last term of Eq. (1) is responsible for the tilt of the Dirac cones in the y-direction. Also, $v_x \neq v_y$ and $v_t \neq 0$ imply that the constant-energy contours on the Dirac cones are elliptical, which are different from circular ones in pristine graphene ($v_x = v_y$, $v_t = 0$).

If the system is further subjected to a uniform static magnetic field $\vec{B} = (0, 0, B)$ and a dc electric field $\vec{E} = (E_r, 0, 0)$. The low energy one-electron effective Hamiltonian reads [45]

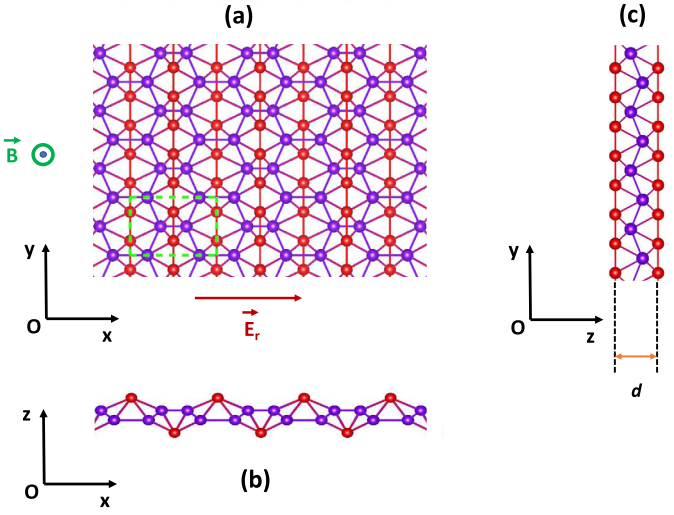

Fig. 1. A 8–*Pmmn* borophene monolayer with the top view (a) and side views (b,c). Two kinds of nonequivalent boron atoms are distinguished by two different colors. The rectangle in Fig. 1(a) indicates the unit cell containing eight boron atoms. (For interpretation of the colors in the figure(s), the reader is referred to the web version of this article.)

$$\mathcal{H} = \xi\left[v_x p_x \sigma_x + v_y(p_y + eBx)\sigma_y + v_t(p_y + eBx)\mathbb{1}\right] + eE_r x\mathbb{1}, \tag{2}$$

in which the Peierls substitution, $\vec{p} \to \vec{p} + e\vec{A}$, has been used with $\vec{A}$ being the magnetic vector potential given in the Landau gauge as $\vec{A} = (0, Bx, 0)$. The eigenfunction-eigenvalue problem of the Hamiltonian (2) has been solved analytically and presented in detail in Ref. [45] and references therein. In this work, we focus on the optical absorption properties of the system stimulated by an external electromagnetic wave so we simply write out directly the solutions obtained before for this problem. In the rest frame, the eigenvalues of the Hamiltonian (2) can be expressed as

$$E_\zeta = \lambda\hbar\omega_c\sqrt{2n}\left(1-\beta_\xi^2\right)^{3/4} - \hbar v_e k_y, \tag{3}$$

and the corresponding eigenfunctions are [45]

$$\Psi_\zeta(\vec{r}) = \frac{e^{ik_y y}}{\sqrt{2L_y\gamma_\xi}}\Big[\begin{pmatrix}\cosh(\theta_\xi/2)\\ -i\sinh(\theta_\xi/2)\end{pmatrix}\lambda\phi_n(X') - i\xi\begin{pmatrix}-i\sinh(\theta_\xi/2)\\ \cosh(\theta_\xi/2)\end{pmatrix}\phi_{n-1}(X')\Big], \tag{4}$$

where $\zeta = \{n, \xi, \lambda, k_y\}$, $\lambda = +1(-1)$ for the conduction (valance) band, $n = 1, 2, 3, \ldots$ is the index of Landau levels (LLs), k_y and L_y are, respectively, the wave vector component and normalization length along the y-direction, $\vec{r} = (x, y)$ is the 2D position vector of carrier, $v_e = E_r/B$, $\beta_\xi = v_e^\xi/\sqrt{v_x v_y}$, $v_e^\xi = v_e + \xi v_t$, $\gamma_\xi = 1/\sqrt{1-\beta_\xi^2}$, $\omega_c = v_c/l_c$ is the cyclotron frequency with $v_c = \sqrt{v_x v_y}$ and $\ell_c = \sqrt{\hbar/eB}$ being the magnetic length, $\phi_n(X')$ is the well known harmonic oscillator wave functions with the argument $X' = \frac{(1-\beta_\xi^2)^{1/4}}{\ell_c}\left[x + k_y\ell_c^2 + \lambda\frac{\sqrt{2n}\ell_c\beta_\xi}{(1-\beta_\xi^2)^{1/4}}\right]$, and the angle θ_ξ is determined by $\tanh\theta_\xi = \beta_\xi$.

The problem for the ground state ($n = 0$) is treated separately. The eigenfunction for this state is given by

$$\Psi_{\{0,\xi,k_y\}}(\vec{r}) = \frac{e^{ik_y y}}{\sqrt{2L_y\gamma_\xi}}\Big[\lambda\begin{pmatrix}\cosh(\theta_\xi/2)\\ -i\sinh(\theta_\xi/2)\end{pmatrix}\phi_0(X')\Big], \tag{5}$$

with the corresponding energy $E_{0,k_y} = -\hbar v_e k_y$. The above energy dispersion and wave functions are necessary for calculating the MOAC in the 8–*Pmmn* borophene monolayer when the system is stimulated by an electromagnetic wave (optical field).

2.2. Magneto-optical absorption coefficient in a 8–Pmmn borophene monolayer

Now we consider the propagation of a linearly polarized electromagnetic wave (light wave) of the frequency ω in the above-mentioned 8–*Pmmn* borophene monolayer. We assume that the polarization vector is parallel to the x-axis. Then, the Hamiltonian operator of the electron-photon interaction has the form [46–48]

$$H_R = \frac{-ie\hbar}{m_e}\sqrt{\frac{2\pi\hbar N_f}{\epsilon_0\epsilon_r\omega V_0}}\frac{\partial}{\partial x}, \tag{6}$$

where N_f is the number of photons, ϵ_0 is the vacuum permittivity, ϵ_r is the dielectric constant or the relative permittivity of the material which is taken as $\epsilon_r = 10$ [45], V_0 is the sample volume, and e is the electron charge. In Eq. (6), m_e is referred as the electron effective mass developed previously in Refs. [49,50] and sometimes referred to as the optical effective mass [51], which is applicable for an arbitrary energy dispersion including non-parabolic energy dispersion materials such as graphene or 8-*Pmmn* borophene with linear energy dispersion.

The MOAC, $\Gamma^{(\xi)}$, in the case of a degenerate electron gas can be related to the quatum-mechanical transition probability for the absorption of photon as [47]

$$\Gamma^{(\xi)} = \frac{2\pi\sqrt{\epsilon}}{c\hbar N_f}\sum_{\zeta,\zeta'} f_{E_\zeta}(1-f_{E_{\zeta'}})|\langle\zeta'|H_R|\zeta\rangle|^2\delta(E_\zeta - E_{\zeta'} + \hbar\omega), \tag{7}$$

where c is the light speed in vacuum, f_{E_ζ} is the Fermi distribution function of the degenerate electron gas, $\delta(x)$ is the δ-Dirac function, $\langle\zeta'|H_R|\zeta\rangle$ is the matrix element of H_R. In the dipole approximation, using Eqs. (4) and (6) one can obtain for a particular valley ξ (intra-valley transitions)

$$\begin{aligned}
&\langle n',\xi,\lambda',k_y'|H_R|n,\xi,\lambda,k_y\rangle \\
&= \frac{-ie\hbar}{2m_e\alpha_c}\Big(\frac{2\pi\hbar N_f}{\epsilon_0\epsilon\omega V}\Big)^{1/2}\delta_{k_y,k_y'} \\
&\times\Big[\lambda\lambda'\Big(-\sqrt{\frac{n+1}{2}}\delta_{n',n+1}+\sqrt{\frac{n}{2}}\delta_{n',n-1}\Big) \\
&+\lambda'\xi\beta_\xi\Big(-\sqrt{\frac{n}{2}}\delta_{n',n}+\sqrt{\frac{n-1}{2}}\delta_{n',n-2}\Big) \\
&+\lambda\xi\beta_\xi\Big(-\sqrt{\frac{n+1}{2}}\delta_{n'-1,n+1}+\sqrt{\frac{n}{2}}\delta_{n',n}\Big) \\
&+\Big(-\sqrt{\frac{n}{2}}\delta_{n'-1,n}+\sqrt{\frac{n-1}{2}}\delta_{n',n-1}\Big)\Big],
\end{aligned} \tag{8}$$

for the transitions between non-zero LLs ($n, n' \neq 0$). For the transitions between the zeroth level ($n = 0$ or $n' = 0$) and any other level, we have

$$\begin{aligned}
&\langle n',\xi,\lambda',k_y'|H_R|0,\xi,\lambda,k_y\rangle \\
&= \frac{\lambda\lambda'}{2\sqrt{2}}\frac{ie\hbar}{m_e\alpha_c}\Big(\frac{2\pi\hbar N_f}{\epsilon_0\epsilon\omega V}\Big)^{1/2}\delta_{0,n'-1}\delta_{k_y,k_{y'}},
\end{aligned} \tag{9}$$

where $\alpha_c = \ell_c/(1-\beta_\xi^2)^{1/4}$.

To calculate the MOAC further, we now assume that the effect of k_y through Fermi distribution function is very small and hence we can ignore it [52], i.e., $f_{E_\zeta} = f_{E_{n,\xi,\lambda}}$ with $E_{n,\xi,\lambda} = \lambda\hbar\omega_c\sqrt{2n}\big(1-\beta_\xi^2\big)^{3/4}$. This assumption is well justified for weak electric field. Inserting Eq. (8) into Eq. (7) and transforming the sum $\sum_{k_y}$ into the integral as $\frac{L_y}{2\pi}\int_{-L_x/2\ell_c^2}^{L_x/2\ell_c^2}dk_y$, one can obtain the expression for the MOAC as

$$\begin{aligned}
\Gamma^{(\xi)} &= \frac{\pi e^2\hbar^2(1-\beta_\xi^2)^{1/2}}{2cm_e^2\epsilon_0\sqrt{\epsilon}\omega\ell_c^4 d}\sum_n\Big\{\Big[(n+1/2)f_{E_{n,\xi,\lambda}}(1-f_{E_{n+1,\xi,\lambda'}}) \\
&\times\delta(E_{n,\xi,\lambda}-E_{n+1,\xi,\lambda'}+\hbar\omega) \\
&+(n-1/2)f_{E_{n,\xi,\lambda}}(1-f_{E_{n-1,\xi,\lambda'}})\delta(E_{n,\xi,\lambda}-E_{n-1,\xi,\lambda'}+\hbar\omega)\Big] \\
&+\beta_\xi^2\Big[\frac{n-1}{2}f_{E_{n,\xi,\lambda}}(1-f_{E_{n-2,\xi,\lambda'}})\delta(E_{n,\xi,\lambda}-E_{n-2,\xi,\lambda'}+\hbar\omega) \\
&+\frac{n+1}{2}f_{E_{n,\xi,\lambda}}(1-f_{E_{n+2,\xi,\lambda'}})\delta(E_{n,\xi,\lambda}-E_{n+2,\xi,\lambda'}+\hbar\omega)\Big]\Big\},
\end{aligned} \tag{10}$$

where we have used the relation $|\lambda|^2 = |\lambda'|^2 = 1$ and $d = 2.18$ Å is the vertical thickness of the 8–*Pmmn* borophene monolayer in the z-direction [53].

To carry out the numerical consideration of the MOAC, the δ-Dirac functions will be replaced by the Lorentzian representation as $\delta(E_\zeta - E_{\zeta'} + \hbar\omega) = \pi^{-1}\gamma_0/[\gamma_0^2 + (E_\zeta - E_{\zeta'} + \hbar\omega)^2]$, where γ_0 is the phenomenological broadening parameter. In this calculation, γ_0 is assumed to depend on the magnetic field and in the very weak broadening regime it is taken as $\gamma_0 = 0.05\hbar\omega_c$ [45].

It can be seen from Eq. (10) that transitions satisfying $n' = n \pm 1$ and $n' = n \pm 2$ are allowed. This means that there exist not only optical transitions between adjacent LLs, but also the transitions between next-nearest neighboring ones. This is the consequence of the selection rules stated by the Kronecker symbols in Eq. (8). We will further analyze this feature in the next section (Sec. 3) where we carry out the numerical calculation to clarify the effect of the tilt of the Dirac cones in 8–*Pmmn* borophene and the external in-plane EF on the absorption spectrum.

3. Numerical results and discussion

This section devotes to evaluate numerically the MOAC obtained above to show the behaviors of the absorption spectrum. In this investigation, we consider the intrinsic system where the Fermi level locates at zero energy, the valence band is fully occupied and the conduction band is empty. Then only the inter-band transitions between the valence and conduction band are considered, i.e., $\lambda = -1$ and $\lambda' = +1$. It should be noted that although the Fermi energy fluctuates weakly between nearest LLs with respect to the magnetic field in reality [32], however, we can keep it constant in the following as the fluctuation amplitude is very small. Before delving into the analysis of the results it is worth spending some words on the role of v_t and E_r in determining the β_ξ involved in Eqs. (3) and (10), that makes the LLs and MOAC in 8–*Pmmn* borophene different from it is in some 2D materials such as graphene, silicene and germanene. Recall that $\beta_\xi = (v_e + \xi v_t)/v_c$, so if we take for instance, $E_r = 10^3$ V m^{-1} and $B = 0.3$ T, then $v_e = E_r/B \approx 3.33\times10^3$ m s^{-1}, which is about one hundred times smaller than the tilt velocity v_t ($= 0.32\times10^6$ m s^{-1}). This indicates that in the very weak electric field limit, the contribution of v_e to the coefficient β_ξ is very small and the sign of β_ξ is dominant by the valley index ξ ($+1$ or -1). This behavior becomes more evident when the magnetic field is stronger. All the following results are obtained at low temperature of 4.2 K, which is a typical value and suitable for the assumption of a degenerate electron gas. One can also take the limit $T \to 0$ and see that the results for the MOAC are still qualitatively conserved.

3.1. Effect of the tilt of Dirac cones

We first investigate the effect of the tilt of Dirac cones on the absorption spectrum. To do so, here we consider $v_t = 0.32v_0$ and $v_t = 0$ to compare between 8–*Pmmn* borophene and other 2D Dirac materials with non-tilted (normal) Dirac cones. In Fig. 2, we

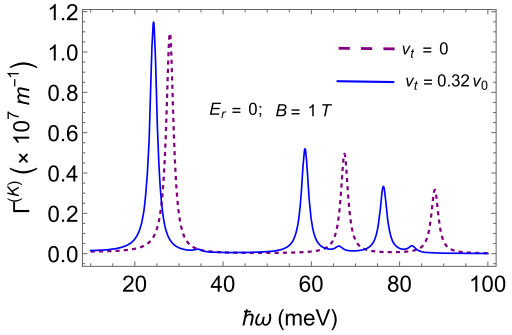

Fig. 2. Dependence of the MOAC on the photon energy in the valley K at two values of the tilt velocity when the in-plane EF is absent ($E_r = 0$). Here, the LLs $n = 0 \div 2$ are taken.

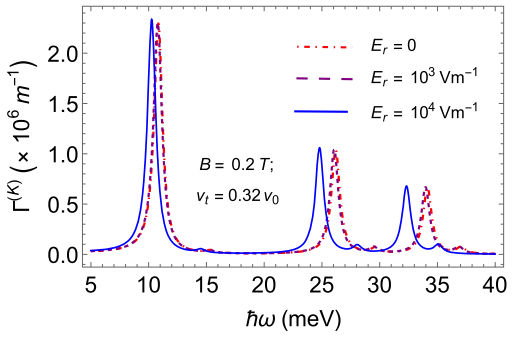

Fig. 3. Dependence of the MOAC on the photon energy in the valley K at different values of in-plane EF.

plot the MOAC in valley K ($\xi = +1$) as a function of the photon energy at $B = 1$ T in the absence of the in-plane EF ($E_r = 0$). In both cases of v_t, there are principal absorption peaks in the MOAC with the absorption intensities being of the same order with those obtained before in silicene and germanene in the same range of magnetic field strength [39]. These peaks arise due to the optical transitions of electrons from the valence band to the conduction band between the LLs n and $n \pm 1$, guaranteed by the matrix element in Eq. (8), similar to those observed in graphene [38], silicene [39,55], germanene [39], phosphorene [40], topological insulators [56], and the TMDs monolayers [42,43]. In each curve, the highest peak (the first one on the left) is referred to the transitions between the zeroth LL ($n = 0$) and the first LL ($n = 1$). The second and the third peaks, respectively, correspond to the contributions of transitions between LLs $1 \leftrightarrow 2$ and $2 \leftrightarrow 3$. Of course, there will be more peaks in the absorption spectrum if we consider larger LL indices in the calculation, as observed for silicene and germanene [39]. However, we limit ourself here to take into account only the transitions between some first LLs because as the LL index increases the peak intensity is reduced rapidly. Another reason is that our main aim here is to clarify the effect of the tilt of the Dirac cones in 8–$Pmmn$ borophene. We now pay our attention to the absorption curve with $v_t \neq 0$. It can be seen clearly from the figure that the non-zero tilt velocity causes the shift of the absorption peaks to the lower photon energy. In the other words, the appearance of the tilt velocity results in a redshift of the peaks. This is because the principal peaks satisfy the conditions $\hbar\omega = E_{n\pm1,+1,+1} - E_{n,+1,-1} = \sqrt{2}(\sqrt{n \pm 1} + \sqrt{n})(1 - \beta_\xi^2)^{3/4}\hbar\omega_c \equiv \Delta E$. It is clear that, for a given LL index n, the presence of the tilt velocity leads to a non-zero β_ξ even $E_r = 0$, and accordingly ΔE is smaller than it is for non-tilted case with $v_t = 0$ and $\beta_\xi = 0$, leading to a shift of the peaks towards low $\hbar\omega$.

An interesting point can be seen also in the curve with $v_t \neq 0$ in Fig. 2 is that there exist minor additional absorption peaks nearby the principal ones. These minor peaks arise due to the transitions between the LLs n and $n \pm 2$ mentioned before in Sec. 2. This kind of transitions between next-nearest neighboring LLs was predicted in type-II Weyl semimetals with tilted Dirac cones [54] and has not been observed before in the magneto-optical absorption in pristine 2D materials with non-tilted Dirac cones such as graphene, silicene, germanene, phosphorene, and so on. Mathematically, the contribution of these transitions to the MOAC is expressed by the terms within the second square brackets in Eq. (10) which are proportional to β_ξ^2. It is seen that in the absence of in-plane EF, $\beta_\xi^2 \neq 0$ only if the tilt velocity v_t is non-zero, namely these transitions occur due to the tilt of the Dirac cones in 8–$Pmmn$ borophene monolayer and are not observed in graphene, silicene and germanene with non-tilted Dirac cones ($v_t = 0$). It is worthwhile to mention that optical transitions between next-nearest neighboring LLs have been observed in MoS_2 monolayer [57] in which the authors calculated the magnetic field dependent two-photon absorption coefficient. However, the authors indicated that happen only when electron absorbs two photons with the aid of an intermediate virtual state.

3.2. Effect of the in-plane electric field

Having considered the effect of the tilt of Dirac cones, we now turn to the investigation of the effect of the in-plane dc electric field on the MOAC. The effect of in-plane EF is mathematically expressed through the term β_ξ, which modifies the LLs and accordingly the absorbed photon energy via the selection rules.

Fig. 3 shows the dependence of MOAC in the K valley on the photon energy at different values of EF and $v_t = 0.32v_0$. It can be seen that the in-plane EF does not change the shape of the absorption spectrum but shifts the absorption peaks. Also, the stronger the electric field, the farther the peaks shift. To examine and compare how the in-plane EF affects the absorption spectrum in absence and presence of v_t, in each valley K and K', we now focus on the highest peak corresponding to the transitions $0 \leftrightarrow 1$ and show it in Fig. 4 with different scenarios of E_r and v_t. Figs. 4(a,b,c) show that in the absence of in-plane EF and/or tilt velocity, there is no difference in the MOAC between two valleys K and K'. This implies a valley degeneracy in the MOAC. However, as we simultaneously consider a non-zero v_t and switch on the electric field in Fig. 4(d), there appears a significant difference in MOAC between the two valleys indicating the valley-dependent absorption spectrum. We can explain the above observations as follows. The dependence of MOAC on the valley index is expressed through the term β_ξ^2 appearing in Eq. (10) and in the LLs separation (ΔE) therein. Recall that $\beta_\xi^2 = (E_r/B + \xi v_t)^2/v_c^2$. In the case $E_r = 0$ and $v_t \neq 0$ as in Fig. 4(c), $\beta_\xi^2 = v_t^2/v_c^2$ independent of $\xi = +1$ or -1 for the valley K or K', respectively. If we take $E_r \neq 0$ and $v_t = 0$ (Fig. 4(b)), then $\beta_\xi^2 = v_e^2/v_c^2$ with $v_e = E_r/B$, showing no difference between two valleys. The same feature is obtained for the two valleys if we consider $E_r = 0$ and $v_t = 0$ in Fig. 4(a). However, if both E_r and v_t are non-zero, we then have $\beta_{\xi=+1}^2 = (E_r/B + v_t)^2/v_c^2$ differing from $\beta_{\xi=-1}^2 = (E_r/B - v_t)^2/v_c^2$, indicating the dependence of MOAC on the valley degree of freedom, as demonstrated in Fig. 4(d). The above results show that, to achieve the valley polarization in the MOAC it is necessary to take into account simultaneously both the tilt velocity in 8–$Pmmn$ borophene and the in-plane EF. In other words, the presence of in-plane EF in 8–$Pmmn$ borophene causes the lifting of the valley degeneracy in the LLs, leading to the separation of the MOAC peaks in two valleys. In the next subsection, we will numerically calculate the valley polarization in the MOAC and analyze its dependence on the external electromagnetic fields.

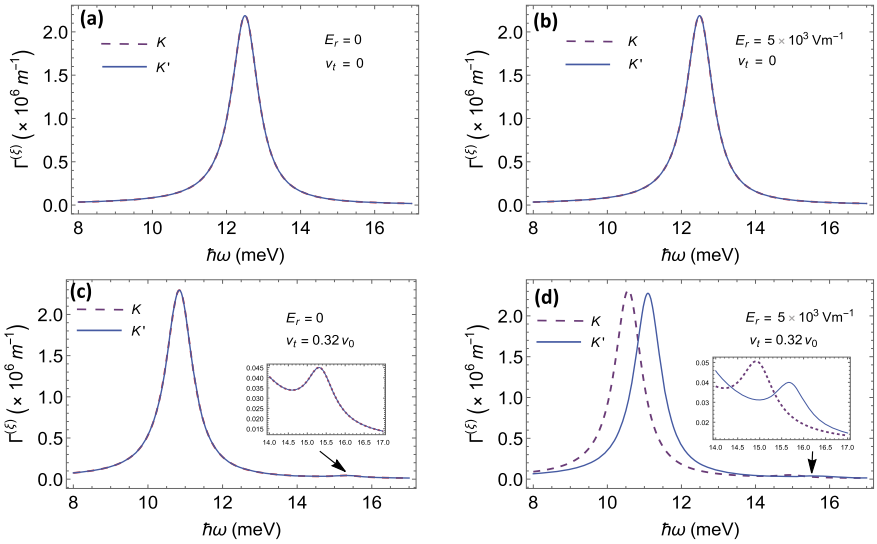

Fig. 4. The MOAC versus photon energy for different scenarios of the in-plane EF and the tilt velocity. Here, $B = 0.2$ T.

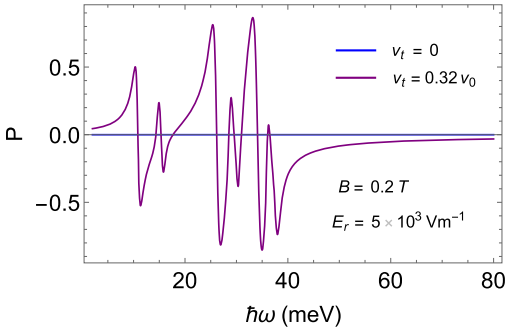

Fig. 5. The valley polarization in the MOAC versus the photon energy for two cases: ignoring and including the tilt velocity.

3.3. The valley polarization versus external fields

We now define the valley polarization in the MOAC as

$$P = \frac{\Gamma^{(K)} - \Gamma^{(K')}}{\Gamma^{(K)} + \Gamma^{(K')}}. \tag{11}$$

Here, we recall that $K(K')$ corresponds to $\xi = +1(-1)$. In Fig. 5, we plot P versus the photon energy at $v_t = 0$ and $v_t = 0.32v_0$. It is seen that there is no valley polarization ($P = 0$) if we ignore the tilt velocity ($v_t = 0$) even in the presence of in-plane EF. This is in accordance with the results in Figs. 4(a) and 4(b) above. On the contrary, when $v_t = 0.32v_0$ is included the valley polarization appears clearly in the range of photon energy from 10 to 40 meV for the given B and E_r. We also see the oscillation in the polarization versus photon energy. This can be explained by the oscillatory nature of the MOAC with photon energy in both valleys, shown in Figs. 2 and 3.

In Fig. 6, the dependence of valley polarization on the magnetic field and in-plane EF is shown. Figs. 6(a) and 6(b) indicate that P is always zero in the absence of the in-plane EF ($E_r = 0$) or the tilt velocity ($v_t = 0$). This confirms once again the observations in Figs. 4(a,b,c). When the in-plane EF of 5 kV m^{-1} is switched on in Fig. 6(a), the sizable valley polarization can be achieved for the magnetic field region smaller than 0.5 T. The polarization amplitude is smaller when the in-plane EF is weaker, as seen in the curve for $E_r = 2$ kV m^{-1}. The oscillatory behavior of P with the magnetic field in Fig. 6(a) originates from the oscillatory nature of MOAC versus magnetic field, like it is versus the photon energy. The competitive roles of B and E_r in determining the value of P can be mathematically understood via β_ξ^2 in $\Gamma^{(\xi)}$. As mentioned in the previous subsection 3.2, $\beta_\xi^2 = (v_e + \xi v_t)^2/v_c^2$ with $v_e = E_r/B$. Thus, if B and E_r are chosen such that $v_e \ll v_t$ (or $v_e = 0$ as $E_r = 0$), then $\beta_\xi^2 \approx (\xi v_t)^2/v_c^2 = v_t^2/v_c^2$ for both $\xi = +1$ and -1, so the degeneracy of two valleys remains and the MOAC is not polarized. However, if we take the values of E_r and B such that v_e value has the same order of or equal to v_t, then β_{+1}^2 and β_{-1}^2 are considerably different, resulting in the large valley polarization. This behavior is verified once again in Fig. 6(b) where the evolution of polarization with in-plane EF is plotted at $B = 0.2$ T. For the magnetic field of 0.2 T, the valley polarization is achieved significantly with the in-plane EF larger than 0.5 kV m^{-1}. Also, in the range of in-plane EF in the figure, there is a maximum value in the polarization. The value of E_r at which P is maximum is the one such that β_{+1}^2 and β_{-1}^2 differ the most. For a more general view, in Fig. 7 we show the density plot of the valley polarization versus magnetic field and in-plane EF where the photon energy of 33 meV is considered. This photon energy is taken in order to be consistent with the range observed in Figs. 2 to 5, where the optical transitions and valley polarization emerge strongly. It is seen that with the in-plane EF up to 10 kV m^{-1}, the polarization is well achieved when the magnetic field is less than 0.5 T. This can be understood by using the relation between the absorbed photon energy and magnetic field (via $\hbar\omega_c$) at the peaks, that is $\hbar\omega = \sqrt{2}(\sqrt{n \pm 1} + \sqrt{n})(1 - \beta_\xi^2)^{3/4}\hbar\omega_c$ with $\omega_c = v_c/\sqrt{\hbar(eB)^{-1}}$. From this relation, one can deduce that for the magnetic field considered less than 0.5 T, the optical transitions between the first LLs take place at photon energies of a few tens of meV, that are in accordance with those in Fig. 3. That is why we choose $\hbar\omega = 33meV$ in the calculation of Fig. 7. The observation also indicates that for those ranges of magnetic field and in-plane EF, the valley polarization in MOAC is most clearly observed when using electromagnetic wave in the far infrared region. We can also use electromagnetic wave with higher photon energy to achieve the polarization if we use stronger magnetic fields. Then, the in-plane EF must be strengthened in order to keep the value of v_e ($= E_r/B$) in combination with $v_t \neq 0$ can cause expected polarization. Theoretically, however, we should not use too strong EF to guarantee that the assumption of k_y-independent Fermi distribution and the linear response are still valid. It is worth mentioning that in the work [52] on the quantum Hall effect in graphene, the Kubo–Greenwood formula within linear response theory and the assumption of k_y-

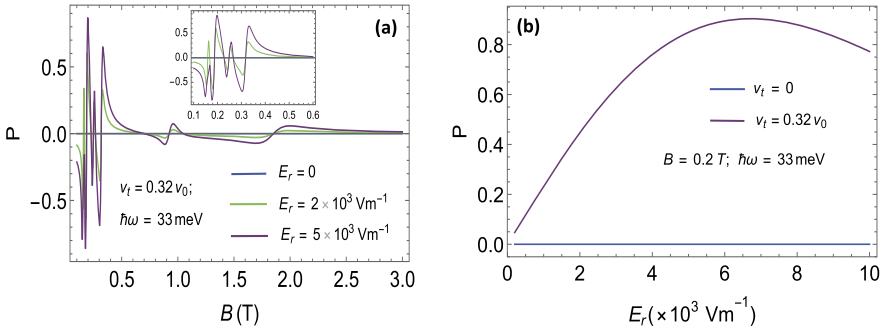

Fig. 6. The valley polarization in the MOAC versus the magnetic field (a) and in-plane EF (b).

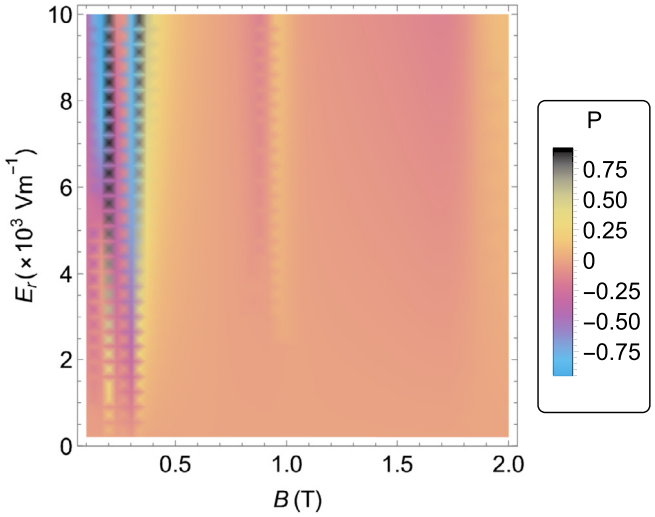

Fig. 7. The density plot of valley polarization versus the magnetic field and in-plane EF.

independent Fermi distribution were applicable for the in-plane electric field up to 100 kV m^{-1}.

4. Concluding remarks

We have carried out a theoretical study of the magneto-optical absorption in a 2D 8–*Pmmn* borophene monolayer with the naturally tilted Dirac cones, subjected to perpendicular magnetic field and external in-plane EF. The MOAC has been calculated in the framework of the perturbation theory. Important results can be summarized as follows.

The presence of the tilt parameter/velocity ($v_t \neq 0$) in 8–*Pmmn* borophene leads to additional optical transitions between LLs n and $n \pm 2$, described by the minor peaks in the absorption spectrum beside principal peaks corresponding to the transitions between LLs n and $n \pm 1$. The transitions between next-nearest neighboring LLs, i.e., LLs n and $n \pm 2$, were not observed before in 2D materials with non-tilted Dirac cones such as pristine graphene, silicene, germanene, and so on. This result opens the possibility to detect the tilt parameter in Dirac materials via the magneto-optical absorption spectrum.

In the absence of external in-plane EF ($E_r = 0$) and/or the tilt parameter ($v_t = 0$) the valley degeneracy of LLs remains and the valley polarization in MOAC does not occur. In contrast, the simultaneous presence of both in-plane EF and the tilt parameter in 8–*Pmmn* borophene removes the valley degeneracy of LLs and accordingly causes the valley polarization in the MOAC. One can be able to control the valley polarization by varying the values of magnetic field, in-plane EF and photon energy accordingly. For instance, if the magnetic field less than 0.5 T, the in-plane EF value should be of the order of kV m^{-1} and the photon energy should be in the range of several tens of meV for good polarization to be observed. The present observations are of importance for applications in valleytronic devices operating in different light regions.

CRediT authorship contribution statement

Ta T. Tho: Writing – review & editing, Writing – original draft, Software, Investigation, Funding acquisition, Formal analysis, Data curation. **Nguyen N. Hieu:** Writing – review & editing, Writing – original draft, Visualization, Software, Investigation, Formal analysis, Data curation. **Doan M. Quang:** Writing – review & editing, Writing – original draft, Investigation, Formal analysis, Data curation. **Nguyen Q. Bau:** Writing – review & editing, Writing – original draft, Visualization, Software, Investigation, Formal analysis. **Bui D. Hoi:** Writing – review & editing, Writing – original draft, Visualization, Methodology, Investigation, Formal analysis, Data curation, Conceptualization.

Declaration of competing interest

The authors declare that they have no known competing financial interests or personal relationships that could have appeared to influence the work reported in this paper.

Data availability

Data will be made available on request.

Acknowledgements

This research is funded by Hanoi University of Civil Engineering under grant number 29-2021/KHXD-TD.

References

[1] K.S. Novoselov, A.K. Geim, S.V. Morozov, D. Jiang, Y. Zhang, S.V. Dubonos, I.V. Grigorieva, A.A. Firsov, Science 306 (2004) 666.
[2] A.K. Geim, Science 324 (2009) 1530.
[3] C.-C. Liu, H. Jiang, Y. Yao, Phys. Rev. B 84 (2011) 195430.
[4] M. Ezawa, Phys. Rev. Lett. 109 (2012) 055502.
[5] M. Derivaz, D. Dentel, R. Stephan, M.-C. Hanf, A. Mehdaoui, P. Sonnet, C. Pirri, Nano Lett. 15 (2015) 2510.
[6] F.-f. Zhu, W.-j. Chen, Y. Xu, C.-l. Gao, D.-d. Guan, C.-h. Liu, D. Qian, S.-C. Zhang, J.-f. Jia, Nat. Mater. 14 (2015) 1020.
[7] Y. Xu, B. Yan, H.-J. Zhang, J. Wang, G. Xu, P. Tang, W. Duan, S.-C. Zhang, Phys. Rev. Lett. 111 (2013) 136804.
[8] A. Splendiani, L. Sun, Y. Zhang, T. Li, J. Kim, C.-Y. Chim, G. Galli, F. Wang, Nano Lett. 10 (2010) 1271.
[9] C. Kamal, A. Chakrabarti, M. Ezawa, New J. Phys. 17 (2015) 083014.
[10] C. Kamal, M. Ezawa, Phys. Rev. B 91 (2015) 085423.
[11] S. Zhang, Z. Yan, Y. Li, Z. Chen, H. Zeng, Angew. Chem., Int. Ed. 54 (2015) 3112.
[12] I.K. Drozdov, A. Alexandradinata, S. Jeon, S. Nadj-Perge, H. Ji, R.J. Cava, B. Andrei Bernevig, A. Yazdani, Nat. Phys. 10 (2014) 664.

[13] L. Li, Y. Yu, G.J. Ye, Q. Ge, X. Ou, H. Wu, D. Feng, X.H. Chen, Y. Zhang, Nat. Nanotechnol. 9 (2014) 372.
[14] H. Liu, A.T. Neal, Z. Zhu, Z. Luo, X. Xu, D. Tománek, P.D. Ye, ACS Nano 8 (2014) 4033.
[15] F. Xia, H. Wang, Y. Jia, Nat. Commun. 5 (2014) 4458.
[16] I. Boustani, Surf. Sci. 370 (1997) 355.
[17] M.H. Evans, J.D. Joannopoulos, S.T. Pantelides, Phys. Rev. B 72 (2005) 045434.
[18] H. Tang, S. Ismail-Beigi, Phys. Rev. Lett. 99 (2007) 115501.
[19] X. Wu, J. Dai, Y. Zhao, Z. Zhuo, J. Yang, X.C. Zeng, ACS Nano 6 (2012) 7443.
[20] E.S. Penev, S. Bhowmick, A. Sadrzadeh, B.I. Yakobson, Nano Lett. 12 (2012) 2441.
[21] H. Liu, J. Gao, J. Zhao, Sci. Rep. 3 (2013) 3238.
[22] Y. Liu, E.S. Penev, B.I. Yakobson, Angew. Chem., Int. Ed. 52 (2013) 3156.
[23] Z. Zhang, Y. Yang, G. Gao, B.I. Yakobson, Angew. Chem., Int. Ed. 54 (2015) 13022.
[24] C. Ozdogan, S. Mukhopadhyay, W. Hayami, Z.B. Guvenc, R. Pandey, I. Boustani, J. Phys. Chem. C 114 (2010) 4362.
[25] A.J. Mannix, X.-F. Zhou, B. Kiraly, J.D. Wood, D. Alducin, B.D. Myers, X. Liu, B.L. Fisher, U. Santiago, J.R. Guest, M.J. Yacaman, A. Ponce, A.R. Oganov, M.C. Hersam, N.P. Guisinger, Science 350 (2015) 1513.
[26] B. Feng, J. Zhang, Q. Zhong, W. Li, S. Li, H. Li, P. Cheng, S. Meng, L. Chen, K. Wu, Nat. Chem. 8 (2016) 563.
[27] X.-F. Zhou, X. Dong, A.R. Oganov, Q. Zhu, Y. Tian, H.-T. Wang, Phys. Rev. Lett. 112 (2014) 085502.
[28] F. Ma, Y. Jiao, G. Gao, Y. Gu, A. Bilic, Z. Chen, A. Du, Nano Lett. 16 (2016) 3022.
[29] A. Lopez-Bezanilla, P.B. Littlewood, Phys. Rev. B 93 (2016) 241405(R).
[30] M.O. Goerbig, J.-N. Fuchs, G. Montambaux, F. Piechon, Phys. Rev. B 78 (2008) 045415.
[31] M. Trescher, B. Sbierski, P.W. Brouwer, E.J. Bergholtz, Phys. Rev. B 91 (2015) 115135.
[32] S.F. Islam, A.M. Jayannavar, Phys. Rev. B 96 (2017) 235405.
[33] S.-H. Zhang, W. Yang, Phys. Rev. B 97 (2018) 235440.
[34] S. Verma, A. Mawrie, T.K. Ghosh, Phys. Rev. B 96 (2017) 155418.
[35] K. Sadhukhan, A. Agarwal, Phys. Rev. B 96 (2017) 035410.
[36] V.G. Ibarra-Sierra, J.C. Sandoval-Santana, A. Kunold, G.G. Naumis, Phys. Rev. B 100 (2019) 125302.
[37] Saul A. Herrera, Gerardo G. Naumis, Phys. Rev. B 100 (2019) 195420.
[38] V.P. Gusynin, S.G. Sharapov, J.P. Carbotte, Phys. Rev. Lett. 98 (2007) 157402.
[39] Do Muoi, Nguyen N. Hieu, Chuong V. Nguyen, Bui D. Hoi, Hieu V. Nguyen, Nguyen D. Hien, Nikolai A. Poklonski, S.S. Kubakaddi, Huynh V. Phuc, Phys. Rev. B 101 (2020) 205408.
[40] M. Tahir, P. Vasilopoulos, F.M. Peeters, Phys. Rev. B 92 (2015) 045420.
[41] Nguyen D. Hien, et al., Phys. Rev. B 101 (2020) 045424.
[42] M. Tahir, P. Vasilopoulos, F.M. Peeters, Phys. Rev. B 93 (2016) 035406.
[43] M. Tahir, P. Vasilopoulos, Phys. Rev. B 94 (2016) 045415.
[44] A.D. Zabolotskiy, Y.E. Lozovik, Phys. Rev. B 94 (2016) 165403.
[45] S.K. Firoz Islam, J. Phys. Condens. Matter 30 (27) (2018) 275301.
[46] V.V. Karpunin, V.A. Margulis, Opt. Spectrosc. 122 (6) (2017) 979.
[47] V.V. Karpunin, V.A. Margulis, Semiconductors 53 (4) (2019) 458.
[48] N.G. Galkin, V.A. Margulis, A.V. Shorokhov, Phys. Solid State 43 (3) (2001) 530.
[49] W. Zawadzki, S. Klahn, U. Merkt, Phys. Rev. Lett. 55 (1985) 983.
[50] V. Ariel, arXiv:1205.3995v1 [physics.gen-ph], 2012, https://doi.org/10.48550/arXiv.1205.3995.
[51] K. Seeger, Semiconductor Physics, Springer-Verlag, 1985.
[52] P.M. Krstajic, P. Vasilopoulos, Phys. Rev. B 83 (2011) 075427.
[53] Junhui Yuan, Niannian Yu, Kanhao Xue, Xiangshui Miao, RSC Adv. 7 (2017) 8654.
[54] S. Tchoumakov, et al., Phys. Rev. Lett. 117 (2016) 086402.
[55] C.J. Tabert, E.J. Nicol, Phys. Rev. Lett. 110 (2013) 197402.
[56] Z. Li, J.P. Carbotte, Phys. Rev. B 88 (2013) 045414.
[57] Rui Gong, Chang Zhou, Xiaobo Feng, Phys. Rev. B 105 (2022) 195301.